The link between chemoattractant gradients, developmental signals, and gene expression in social amoebae is elucidated.

Nucleocytoplasmic Shuttling of a GATA Transcription Factor Functions as a Development Timer

Huaqing Cai, Mariko Katoh-Kurasawa, Tetsuya Muramoto, Balaji Santhanam, Yu Long, Lei Li, Masahiro Ueda, Pablo A. Iglesias, Gad Shaulsky, Peter N. Devreotes*
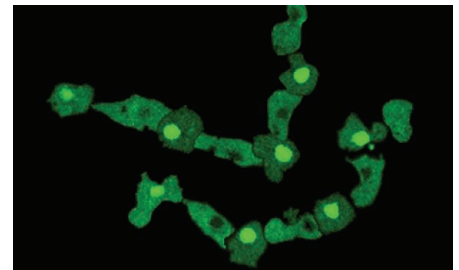
Introduction: Biological oscillations are universally found in nature and are critical at many levels of cellular organization. In the social amoeba *Dictyostelium discoideum*, starvation-triggered cell-cell aggregation and the early stages of developmental morphogenesis are orchestrated by periodic extracellular cAMP (3',5'-cyclic adenosine monophosphate) waves, which provide both chemotactic cues and developmental signals. Repeated occupancy of G protein–coupled cAMP receptors promotes optimal gene expression, whereas continuous stimulation suppresses the program. Although this activity was recognized nearly 40 years ago, the underlying mechanism for the stimulus-response pattern has not been elucidated.

Rationale: We reasoned that the mechanism decoding cyclic stimuli might be traced to a receptor-mediated regulation of a gene that is required for developmental progression. In a genetic screen for mutants that affect proper development, we discovered a GATA family transcription factor, GtaC, which is essential in this process. Furthermore, in different cells at different times, GtaC was found to either accumulate in the nucleus or disperse in the cytosol, suggesting that the dynamic cellular localization of GtaC could be a key to the relay of oscillatory signaling.

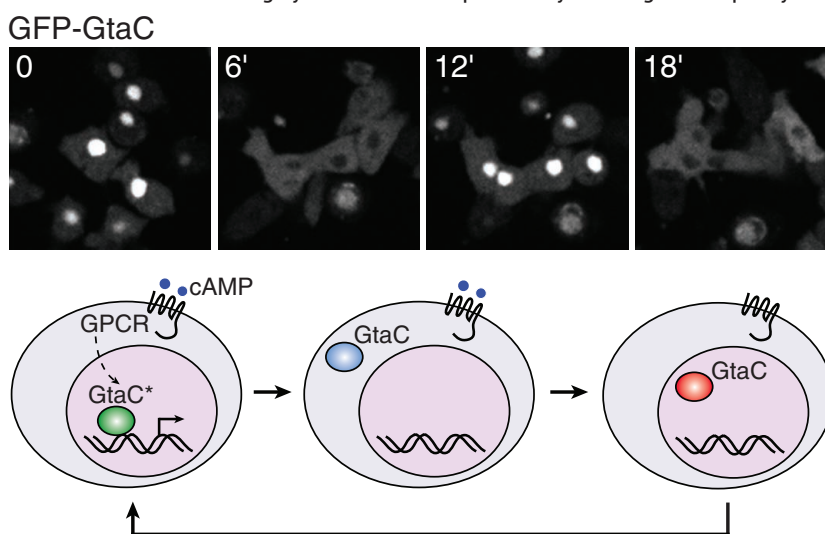**Results:** We report here that GtaC exhibits rapid nucleocytoplasmic shuttling in response to periodic cAMP waves. Persistent occupancy of the receptors by cAMP causes GtaC to translocate and remain out of the nucleus. This behavior requires a negative regulation of an intrinsic nuclear localization signal (NLS) by the N-terminal region of GtaC and

receptor-mediated phosphorylation by the glycogen synthase kinase GskA. When the exit of GtaC from the nucleus is inhibited by adding an exogenous NLS or by mutating the residues involved in phosphorylation, cAMP stimulation, either pulsatile or continuous, induces precocious gene expression and cell differentiation. The two apparently opposing effects of cAMP—it acts as a positive regulator of developmental gene expression but drives GtaC out of the nucleus—suggest that GtaC may be briefly activated during each stimulation cycle before it leaves the nucleus, while its return resensitizes the system. Consistently, we observe that each cAMP cycle generates a transient burst of GtaC-dependent transcription of the contact site A gene (*csaA*), a well-characterized developmental marker. We further demonstrate that this regulatory mechanism enables cells to modulate gene expression by counting low-frequency stimulations but filtering out high-frequency signals; hence, the steady-state expression level of *csaA* is determined by the number of effective cAMP pulses experienced by the cell rather than the concentration of the cAMP stimuli or the overall time since the initiation of development. Computer simulations based on a corresponding logical circuit recapitulate GtaC-mediated accumulation of gene products under various stimulation regimes.

Conclusion: This work reveals a decoding mechanism by which oscillatory signals are used to guide gene expression and promote timely development. Tuning transcription to the number rather than the level of the external

GFP-GtaC

GtaC shuttling modulates developmental gene expression. (**Top**) Periodic nuclear enrichment of GtaC at times indicated in response to cAMP waves. (**Bottom**) In each cAMP stimulation cycle, GtaC transits through successive states of nuclear active (green), cytosolic (blue), and nuclear inactive (red), promoting transcription only in the active state. Repeated stimuli lead to reoccurring activations and incremental accumulation of gene products. The mechanism enables cells to count effective stimuli and modulate gene expression accordingly.

stimuli allows large populations of cells over an expanded territory to be developmentally synchronized. Similar mechanisms may operate in other circumstances where cellular plasticity is linked to repeated experience.

Nucleocytoplasmic Shuttling of a GATA Transcription Factor Functions as a Development Timer

Huaqing Cai,[1] Mariko Katoh-Kurasawa,[2] Tetsuya Muramoto,[3] Balaji Santhanam,[4] Yu Long,[1] Lei Li,[5] Masahiro Ueda,[3,6] Pablo A. Iglesias,[1,7] Gad Shaulsky,[2,4] Peter N. Devreotes[1]*

Biological oscillations are observed at many levels of cellular organization. In the social amoeba *Dictyostelium discoideum*, starvation-triggered multicellular development is organized by periodic cyclic adenosine 3′,5′-monophosphate (cAMP) waves, which provide both chemoattractant gradients and developmental signals. We report that GtaC, a GATA transcription factor, exhibits rapid nucleocytoplasmic shuttling in response to cAMP waves. This behavior requires coordinated action of a nuclear localization signal and reversible G protein (heterotrimeric guanine nucleotide–binding protein)–coupled receptor–mediated phosphorylation. Although both are required for developmental gene expression, receptor occupancy promotes nuclear exit of GtaC, which leads to a transient burst of transcription at each cAMP cycle. We demonstrate that this biological circuit filters out high-frequency signals and counts those admitted, thereby enabling cells to modulate gene expression according to the dynamic pattern of the external stimuli.

Rhythmic phenomena play a critical role in many cellular processes, such as the cell cycle, the circadian clock, the activity of neuronal and cardiac cells, the glycolytic system, and the segmentation of somites. In many cases, the spatiotemporal pattern is as important as the cellular activity itself. For example, the frequency of delivery rather than the total amount governs the physiological efficacy of certain hormones, oscillatory rather than persistent expression of regulatory genes is required for the maintenance of neural progenitor cells, and spaced rather than massed training trials are more reliable at inducing long-term facilitation (1–3).

A fascinating example of biological oscillations occurs in the social amoeba *Dictyostelium discoideum*. In this organism, starvation-triggered chemotactic aggregation and multicellular development are mediated by periodic extracellular cAMP (cyclic adenosine 3′,5′-monophosphate) signals (4, 5). Through the coordinated action of a G protein (heterotrimeric guanine nucleotide–binding protein)–coupled cAMP receptor, an adenylyl cyclase, and phosphodiesterases, self-organized cAMP signals are initiated within aggregation centers and relayed by surrounding cells, resulting in outwardly propagating waves that guide the collective migra-tion of up to 100,000 cells during the early stages of the developmental program. In addition to their role as chemoattractant, the periodic cAMP signals trigger profound changes in the transcriptome (6, 7). It has been known since the 1970s that optimal development is promoted by repeated stimuli at the "correct" frequency and suppressed by continuous stimulation (8, 9), yet the underly-ing mechanism for this pattern of response has been elusive. We report here that developmental progression requires a conserved transcription factor, GtaC, which undergoes oscillatory nucleo-cytoplasmic shuttling. The unique mode of regu-lation of GtaC by extracellular cAMP can explain why correctly timed repeated stimuli are required for proper gene expression and development.

Results

cAMP Waves Drive Oscillatory Nucleocytoplasmic Shuttling of GtaC

In a forward genetic screen using restriction endonuclease–mediated integration (10), we iso-lated a mutant that failed to aggregate when plated clonally on bacteria lawns (fig. S1A). The inser-tion occurred in the second exon of the *gtaC* gene, which encodes a GATA family zinc finger tran-scription factor (fig. S1B), and *gtaC⁻* cells, gen-erated via homologous recombination, recapitulated the phenotype of the original mutant (fig. S1, A and B). When plated on non-nutrient agar, which synchronizes the initiation of development, the aggregation of *gtaC⁻* cells was delayed and im-paired compared to that of wild-type cells (fig. S1C). The application of extracellular pulses of cAMP, which effectively restores development in several aggregationless mutants identified previous-ly (11, 12), failed to rescue development in *gtaC⁻* cells (fig. S1D). The defect was rescued by the ex-pression of green fluorescent protein (GFP)–tagged GtaC, but not GFP-GtaC^{C-S}, in which the four conserved cysteines in the zinc finger domain were mutated to serines (fig. S1, A and C).

An intriguing observation was made when we examined the localization of GFP-GtaC. It underwent oscillatory nucleocytoplasmic shuttling during early development (Fig. 1A and movie S1). This behavior was most apparent 2.5 to 4.5 hours after starvation, a stage when propagating cAMP waves occur (13). On the contrary, little GFP-GtaC was found in the nucleus of growing cells or cells aggregated into moundlike structures later during development (movie S2). The period of shuttling, 6.8 ± 0.6 min, was similar to that re-ported for spontaneous cAMP oscillations (Fig. 1C). Further, whereas shuttling appeared synchro-nized among the cells within a narrow microscopic field (Fig. 1, A and B; fig. S2, A and B; and movie S1), at lower magnification, it became clear that the nuclear localization of GFP-GtaC propagated across the field as a wave with a speed (~100 μm/min) similar to that of cAMP waves (fig. S3 and movie S3) (13, 14). The fact that the rising phase of an approaching cAMP wave causes a transient increase in cell polarity and rate of motility (14, 15) allowed us to align the localization of GtaC with cAMP changes. We observed that the cells be-came slightly elongated and the speed of move-ment increased three- to fourfold when GFP-GtaC localized to the cytoplasm, and they were rounder and less motile when GFP-GtaC was in the nu-cleus (Fig. 1, A and C; fig. S2, A and B; and movie S1). This implies that GtaC shifts to the cytoplasm during the rising phase of the cAMP wave and reenters the nucleus during the falling phase.

To directly assay the effect of cAMP, we mon-itored the behavior of GFP-GtaC in isolated cells during application and removal of stimuli. When exposed to persistent and uniform cAMP stimu-lation, after a brief lag GtaC shifted from the nu-cleus to the cytoplasm with a half-life of ~65 s (Fig. 1D and movie S4) and remained in the cy-toplasm for as long as the stimulus was present (more than 30 min). When the stimulus was re-moved, GtaC reaccumulated in the nucleus with a half-life of ~95 s (Fig. 1D and movie S5). The nucleus-to-cytoplasm translocation depended on cAMP receptor occupancy because it did not oc-cur in cells lacking the receptors cAR1 and cAR3 (Fig. 1D and movie S6). In addition, robust shut-tling could also be observed in cell suspensions when pulses of cAMP were applied at 6-min in-tervals (fig. S2C). Under this condition, each cAMP addition triggered an amplified response, resulting in elevated cAMP levels for about 1 to 2 min, which then declined to basal levels right before the next pulse (16). Consequently, in each stimulation cy-cle, the percentage of cells with nuclear GtaC decreased first, reached a minimum at 3 min, and then returned to the initial level at the end (fig. S2C). Together, these results indicate that nucleo-cytoplasmic shuttling of GtaC is driven by pe-riodic occupancy of the surface receptor from self-organized cAMP oscillations.

[1]Department of Cell Biology, School of Medicine, Johns Hopkins University, Baltimore, MD 21205, USA. [2]Department of Mo-lecular and Human Genetics, Baylor College of Medicine, Houston, TX 77030, USA. [3]Laboratory for Cell Signaling Dynamics, RIKEN Quantitative Biology Center, Osaka 565-0874, Japan. [4]Grad-uate Program in Structural Computational Biology and Mo-lecular Biophysics, Baylor College of Medicine, Houston, TX 77030, USA. [5]Department of Biology, University of Virginia, Charlottesville, VA 22904, USA. [6]Department of Biological Sciences, Graduate School of Science, Osaka University, Osaka 565-0043, Japan. [7]Department of Electrical and Computer En-gineering, Whiting School of Engineering, Johns Hopkins Uni-versity, Baltimore, MD 21218, USA.

*Corresponding author. E-mail: pnd@jhmi.edu

GtaC Shuttling Depends on Its Nuclear Localization Signal and Cyclic Phosphorylation

We constructed a series of mutants to examine the involvement of different regions of GtaC in its dynamic behavior. Because many oscillatory transcription factors reported previously are involved in negative feedback loops where their level or activity is down-regulated by target gene products (*17–20*), we first tested whether shuttling requires the zinc finger DNA binding domain. GFP-GtaC^{C-S} showed no dominant effect when expressed in the wild-type background (fig. S4A), and the kinetics and extent of its nucleo-cytoplasmic relocalization during persistent or repetitive stimulation were indistinguishable from that of the intact protein (Fig. 1D, fig. S2C, and movie S7), indicating that the zinc finger domain is dispensable. In contrast, when a nearby region con-

taining a putative nuclear localization signal (NLS) was deleted (GtaC$^{\Delta NLS}$) or mutated (GtaC^{KR-A}), GtaC could no longer localize to the nucleus or rescue the aggregation defect of *gtaC*$^-$ cells (Fig. 2, A and B, and fig. S4, A and B). Removing most of the C terminus following the zinc finger domain (GtaC$^{\Delta543-587}$) or the N-terminal 180 residues did not significantly impair the localization or function of GtaC (Fig. 2, A and B, and fig. S4, A and B). However, truncations from the N terminus (GtaC$^{\Delta1-228}$, GtaC$^{\Delta1-280}$, and GtaC$^{\Delta1-345}$) led to a complete loss of regulation and constitutive nuclear localization that still depended on the NLS activity (Fig. 2, A and B, and fig. S4B). Because the N-terminal region itself did not have apparent nuclear export activity or consensus sequence (fig. S4C), we speculate that the N terminus of GtaC (involving especially residues 180 to

228) may facilitate cAMP-induced relocalization by neutralizing the action of the endogenous NLS.

We noticed that the nuclear-to-cytoplasmic translocation of GtaC coincided with a shift in its electrophoretic mobility, which required cAMP receptor occupancy (Fig. 2C and fig. S5A). The slower migrating species could be recognized by antibodies to phospho-serine and phospho-threonine, and the shift was reversed by treatment with λ-phosphatase, indicating that it was caused by cAMP-induced phosphorylation (Fig. 2D). Furthermore, periodic changes in the phosphorylation status of GtaC were detected in response to oscillatory cAMP stimulation: GtaC became phosphorylated and then dephosphorylated when levels of cAMP increased and decreased sequentially during each cycle (Fig. 2E). These observations indicate that localization of GtaC is closely linked
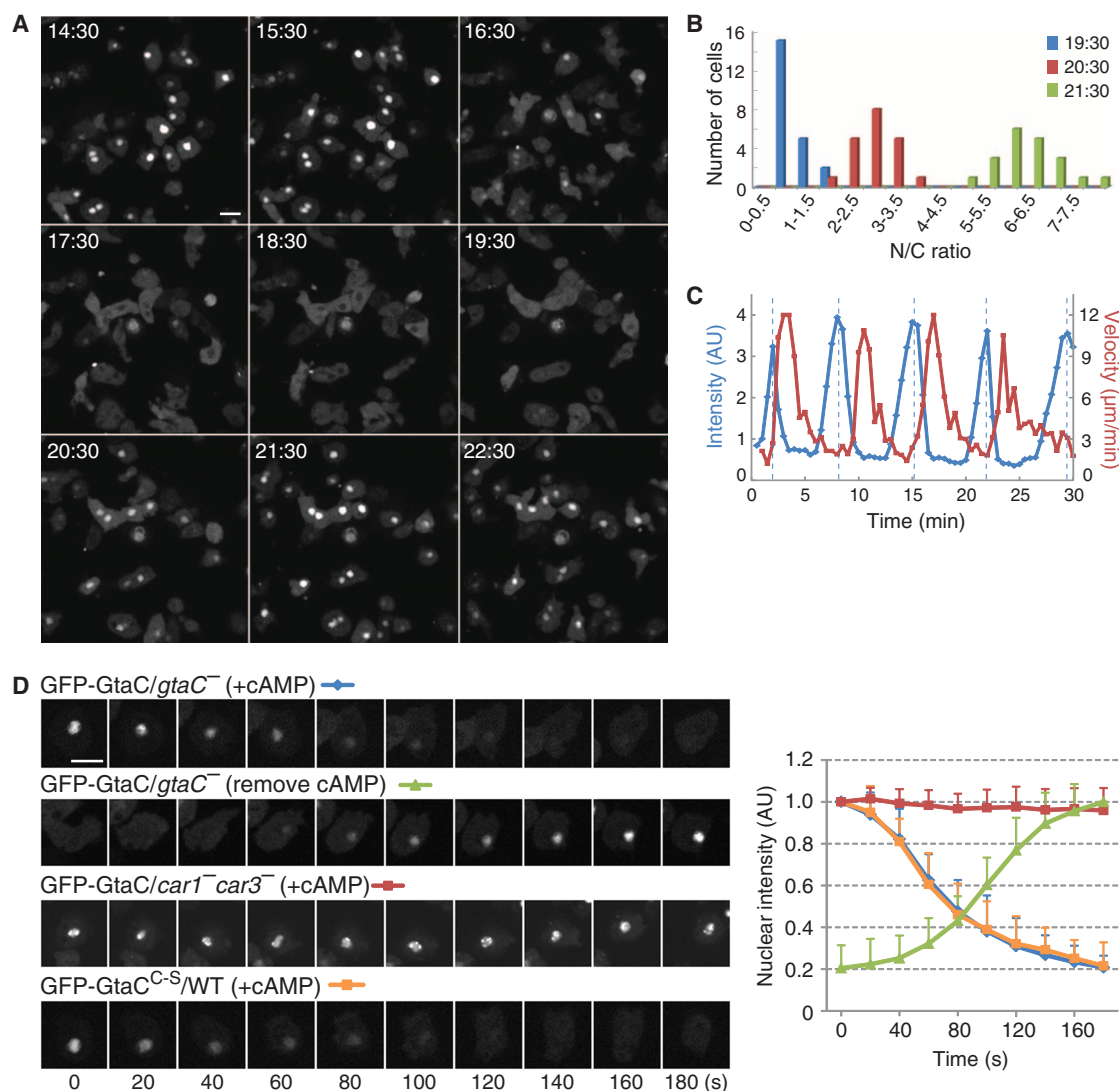
Fig. 1. cAMP oscillations drive the nucleocytoplasmic shuttling of GtaC during early development. (**A**) Time-lapse microscopic images (from movie S1) showing oscillatory nuclear enrichment of GFP-GtaC in a monolayer of cells. Time, minutes:seconds. (**B**) Histogram of the distribution of nucleus/cytoplasm fluorescence intensity ratio (N/C) at the indicated time points. (**C**) Plot of fluorescence intensity of GFP-GtaC (intensity peaks indicated by dashed lines) and speed of cell movement over a 30-min period. (**D**) Image sequence showing nuclear-to-cytoplasmic translocation of GFP-GtaC upon uniform cAMP stimulation (first panel, *n* = 42). The translocation was reversed when a stimulus applied for about 10 min was removed (second panel, *n* = 34), was blocked in cells lacking the cAMP receptors (third panel, *n* = 45), but was not affected by the zinc finger domain mutations (fourth panel, *n* = 40). Quantification of the changes in nuclear fluorescence intensity is shown on the right. Data are means + SD. AU, arbitrary units; WT, wild type. Scale bar, 10 μm.

to its phosphorylation states. Purified phosphorylated and dephosphorylated GtaC displayed different patterns of degradation during limited trypsin digestion, implying a potential conformational change upon phosphorylation (fig. S5B).

To investigate the functional significance of phosphorylation, we sought to map the relevant sites. Two consensus protein kinase A (PKA; effector of intracellular cAMP) recognition sites (S^{472} and T^{473}) were found within the NLS. Alanine substitutions of the two sites, however, did not affect phospho-cycling (fig. S5C). Phosphoproteomic analyses revealed a cluster of three serine/threonine residues (T^{376}, S^{379}, and S^{380}) that were phosphorylated in a cAMP-dependent manner (Fig. 2F). We expressed a construct con-

taining alanine substitutions at these positions as well as mutations in the zinc finger domain ($GtaC^{3A+C-S}$) in the wild-type background. With persistent or repetitive cAMP stimulation, the mutant protein still displayed decreased electrophoretic mobility, but the apparent molecular weight shift was significantly smaller than that displayed by the wild-type protein (Fig. 2, G and H). Furthermore, cAMP-driven nucleocytoplasmic shuttling was impaired (Fig. 2I), confirming the role of the S/T cluster in regulating GtaC localization.

The three mapped phospho-residues are predicted to be recognition sites of two classes of kinases: glycogen synthase kinase 3 (GSK3) and mitogen-activated protein kinase (MAPK). Deleting the two *Dictyostelium* MAPKs, ErkA and ErkB,

had little effect on GtaC phosphorylation (fig. S5D). In contrast, in cells lacking GskA, the homolog of GSK3, the stimulus-induced mobility shift was greatly reduced relative to that observed in the wild-type cells (fig. S5E). Furthermore, by adding purified Flag-GskA in vitro, the full extent of shift could be restored (fig. S5F). Together, these results suggest that the cAMP-induced phosphorylations likely induce conformational changes that coordinate with the N terminus of the protein to counteract the activity of the NLS and promote cytoplasmic localization. Because translocation was not abolished by $GtaC^{3A}$ mutation or disruption of GskA (Fig. 2I and fig. S5G), it may also involve the yet unidentified phosphorylation(s) that produces the residual mobility shift or other regulations.
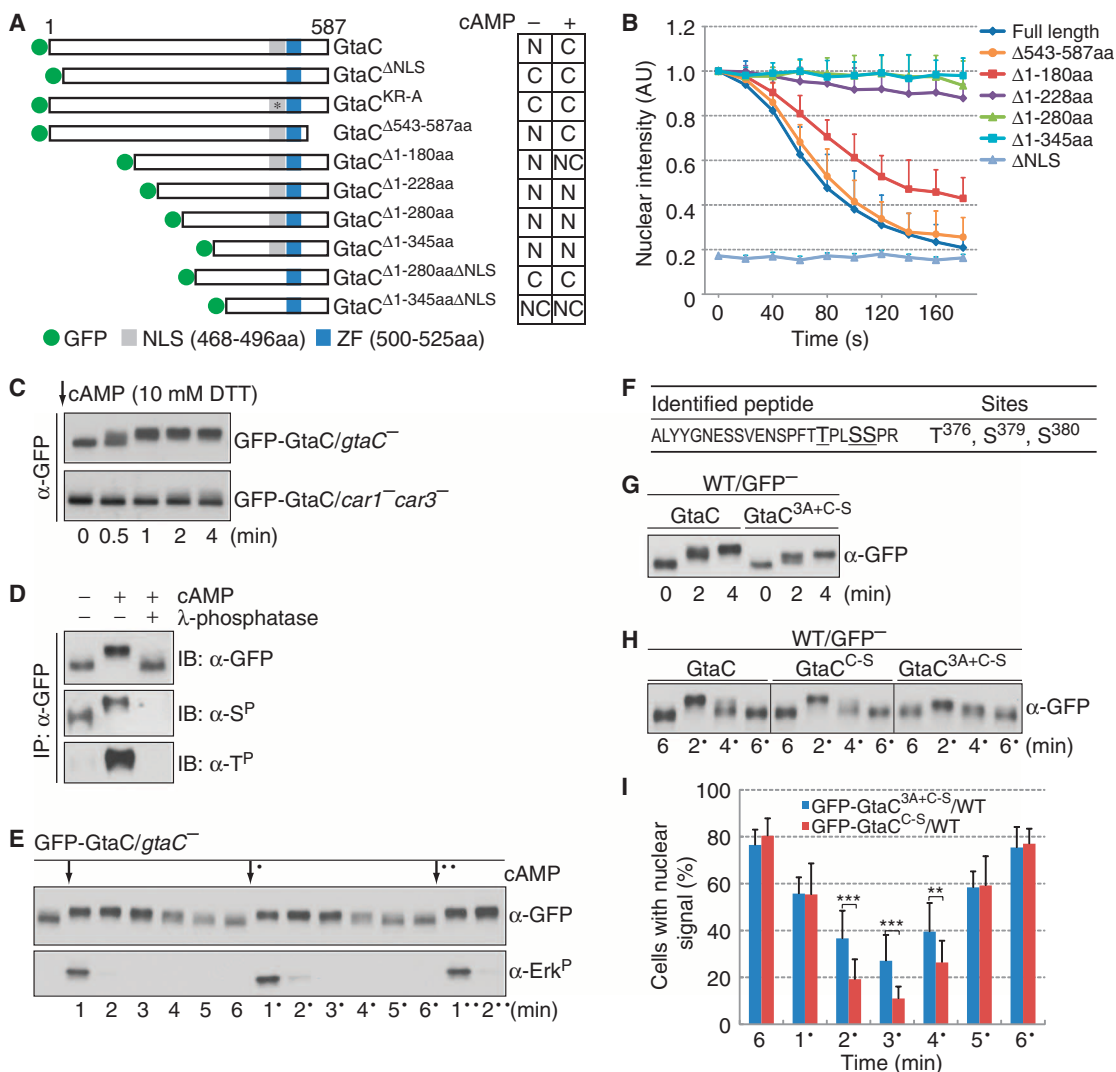
Fig. 2. Regulation of GtaC shuttling. (A) (Left) Schematics of GFP-GtaC and the mutant forms used for localization study. ZF, zinc finger DNA binding domain. Right panel summarizes the localization of WT and mutant proteins before and 5 min after uniform cAMP stimulation (C, predominantly cytoplasmic; N, predominantly nuclear; NC, in both compartments). **(B)** Quantification of the changes in nuclear fluorescence intensity after uniform cAMP stimulation. Data are means + SD ($n \geq 40$). **(C)** Western blot analysis of samples collected after persistent cAMP stimulation [cAMP degradation blocked by dithiothreitol (DTT)]. **(D)** The cAMP-stimulated mobility shift was reversed by treatment with λ-phosphatase. The slower migrating species was recognized by anti-

bodies to phospho-serine and phospho-threonine. **(E)** Pulses of cAMP applied at 6-min intervals (indicated by the arrows) induced periodic changes in the apparent molecular weight of GFP-GtaC and the phosphorylation status of the ErkB kinase (dots by arrows and numbers indicate the pulsing cycle numbers). **(F)** Phosphoproteomic analysis identified three cAMP-dependent phosphorylation sites (underlined). **(G** and **H)** GFP-GtaC^{3A+C-S} displayed reduced mobility shift in response to persistent (G) or pulsatile (H) cAMP stimulation. **(I)** Shuttling of GFP-GtaC^{C-S} and GFP-GtaC^{3A+C-S} in response to pulsatile stimuli. Graph quantitates the percentage of cells with discernible nuclear signal of GtaC. Data are means + SD ($n \geq 150$). **$P < 0.01$; ***$P < 0.001$.

### GtaC Shuttling Regulates Development and Gene Expression

To examine the effects of disrupted shuttling, we added an exogenous NLS, which kept GtaC predominantly in the nucleus (fig. S6A and movie S8). The NLS^{ex}-GFP-GtaC–expressing cells entered development prematurely. When assayed for migration in a defined gradient of cAMP, 2- to 3-hour (post-starvation) NLS^{ex}-GFP-GtaC cells displayed motility and directionality parameters comparable to 4- to 5-hour GFP-GtaC cells (Fig. 3A and movies S9 to S11). Consistently, on non-nutrient agar, NLS^{ex}-GFP-GtaC cells assembled into moundlike structures 2 to 3 hours earlier than wild-type or GFP-GtaC cells (Fig. 3B and fig. S6B). However, the size of these structures, which reflects the number of cells synchronized to aggregate, was greatly reduced and development often arrested at the mound stage (Fig. 3B and fig. S6B).

Rapid and aberrant development was also observed with cells expressing the mutant forms of GtaC (GtaC^{3A}, GtaC$^{\Delta1–228}$, GtaC$^{\Delta1–280}$, and GtaC$^{\Delta1–345}$) that were defective in cAMP-induced translocation (fig. S6C). Moreover, a similar phenotype was reported for $gskA^-$ ([21]), consistent with its demonstrated role in regulating GtaC phosphorylation and translocation (fig. S5, E to G).

To uncover gene expression changes associated with differential development, we performed RNA sequencing (RNA-Seq) analyses with wild-type, $gtaC^-$, GFP-GtaC/$gtaC^-$, and NLS^{ex}-GFP-GtaC/$gtaC^-$ strains (Fig. 3C and fig. S7A). We calculated the maximal correlation between the transcriptional profile of each individual strain and that of the wild type at each development time point using genes whose transcripts exhibited changes in at least one strain ([22]). The initial profiles of all four strains were similar (0 hour in Fig.

3C). The profile of $gtaC^-$ was similar to that of the wild type up to 1 hour of development but arrested thereafter (Fig. 3C), consistent with GtaC being essential for developmental progression (fig. S1). GFP-GtaC/$gtaC^-$ resembled the wild type throughout the time course, suggesting that GFP-GtaC behaved like the endogenous protein and complemented the $gtaC^-$ mutant (Fig. 3C). In contrast, NLS^{ex}-GFP-GtaC markedly accelerated the profile at early time points although it was expressed about two- to threefold lower than GFP-GtaC at the protein level (Fig. 3C). The overall gene expression trends correspond well to the morphological phenotypes of the respective strains (Fig. 3B and fig. S1C).

We then examined developmentally induced transcripts in more detail. Compared to $gtaC^-$, 1008 transcripts exhibited significantly higher abundance at 5 hours in both wild-type and GFP-GtaC/
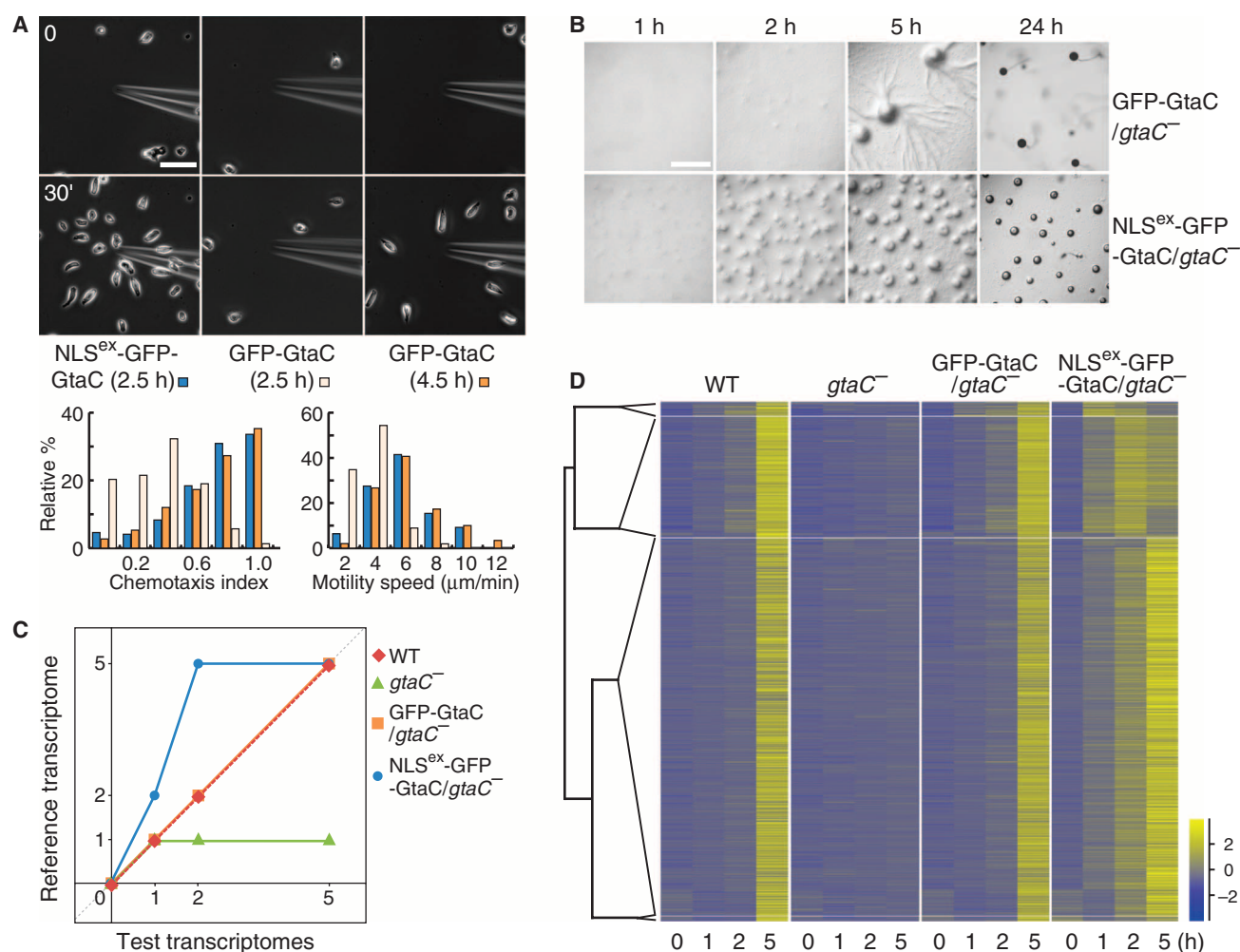
Fig. 3. GtaC shuttling is important for proper gene expression and development progression. (**A**) Cells developed on non-nutrient agar for 2.5 or 4.5 hours were exposed to cAMP gradients generated by a micropipette. (Top) Snapshots taken at the indicated time points. (Bottom) Quantification of chemotaxis index and motility speed ($n \geq 175$). Scale bar, 50 μm. (**B**) Cells expressing NLS^{ex}-GFP-GtaC developed precociously on non-nutrient agar. Scale bar, 2 mm. (**C**) Maximal similarity plot between the four test transcriptomes (WT, $gtaC^-$, GFP-GtaC/$gtaC^-$, and NLS^{ex}-GFP-GtaC/$gtaC^-$) at each development time point (x axis) and the WT reference transcriptome (y axis) generated from

10,280 genes whose transcripts exhibited change in at least one strain. The dashed gray line represents a hypothetical comparison between perfectly matching developmental profiles. (**D**) The heat maps generated from RNA-Seq analyses represent the patterns of change in standardized mRNA abundance of 1008 selected transcripts (rows) over four time points (columns) in the indicated strains. These transcripts were significantly more abundant in WT and GFP-GtaC/$gtaC^-$ cells at 5 hours than in $gtaC^-$ cells. They were grouped by hierarchical clustering analysis on the NLS^{ex}-GFP-GtaC/$gtaC^-$ data over four time points. Colors represent relative mRNA abundances (see scale).

$gtaC^-$ cells, and most of these transcripts (796) were precociously expressed in NLS^{ex}-GFP-GtaC/$gtaC^-$ cells (Fig. 3D). This trend was also found at the 1- and 2-hour time points (fig. S7B). A subset of GtaC-dependent genes (18% in the 1- and 2-hour list and 8% in the 5-hour list) was significantly underexpressed in NLS^{ex}-GFP-GtaC/$gtaC^-$ compared to GFP-GtaC/$gtaC^-$ cells. Gene Ontology (GO) analyses revealed an enrichment of GO terms associated with GtaC-dependent genes, including "cAMP biosynthetic process" and "cell-cell recognition," two essential processes during early development (fig. S7, C to E). Together, these experiments demonstrate that GtaC shuttling is required for proper control of developmental gene expression and development progression.

Nuclear GtaC Is Necessary But Not Sufficient for Development

The persistent nuclear localization rendered by NLS^{ex} enabled further investigation of the requirement of GtaC and cAMP during development. When wild-type or GFP-GtaC/wild-type cells were repeatedly stimulated at 6-min intervals or allowed to oscillate spontaneously, they became polarized and turned on the expression of two GtaC-dependent genes, $csaA$ and $cAR1$, which have been used extensively as markers for development (Fig. 4A and figs. S7, D and E, and S8, A and B). In contrast, continuous stimulation by sp-cAMPS (a nondegradable analog of cAMP) suppressed these events (Fig. 4A and fig. S8, A and B). The suppression by sp-cAMPS could be bypassed by expressing NLS^{ex}-GFP-GtaC (Fig. 4A and fig. S8, A and B). Thus, in wild-type cells, pulses of cAMP are more effective as signals in promoting development than continuous stimuli because the former allow repeated nuclear entry of GtaC, whereas the latter keep GtaC in the cytosol.

To test whether nuclear localization of GtaC alone is sufficient to drive development, we used cells lacking the major adenylyl cyclase (AcaA) that is necessary for cAMP production. In $acaA^-$ cells, which do not have spontaneous oscillations, development and the expression of $csaA$ and $cAR1$ required repeated cAMP stimuli (Fig. 4B and fig. S8C). NLS^{ex}-GFP-GtaC by itself was not able to circumvent this requirement—gene expression and developmental changes did not occur in these cells unless external cAMP stimuli were applied (Fig. 4B and fig. S8C). These experiments indicate that nuclear GtaC is necessary but not sufficient to fully relay cAMP signals and that gene expression needs an additional input from cAMP.

Thus, cAMP signaling appears to play two distinct roles in early development—it acts as a positive regulator of cell differentiation and gene expression but also drives GtaC out of the nucleus and thereby negatively regulates these events. The two seemingly opposing effects encoded in cAMP signaling may allow cells to respond specifically to oscillatory stimuli, which provide a repeated activation signal and repeated nuclear accumulation of GtaC. We carried out experiments to further explore how the dual effects of cAMP allow cells to interpret dynamic signals.

Cells Process Oscillatory cAMP Signaling to Regulate Development

The fact that gene expression responds to repeated stimuli and that GtaC shuttles in and out of the nucleus suggests that transcription may occur in distinct "units." To test this possibility, we used the MS2 technique (fig. S9A) (23, 24), which detects nascent messenger RNA (mRNA) at the site of transcription as a fluorescent spot, to directly visualize transcriptional dynamics of the GtaC-dependent target gene, $csaA$. Remarkably, $csaA$ transcription spots displayed an oscillatory pattern like the cAMP oscillations and GtaC shuttling at the population level (Fig. 5A). They emerged with a period (5.6 ± 0.8 min) similar to that of the nucleocytoplasmic transit of GtaC (5.5 ± 0.1 min) under these conditions (Fig. 5). The peaks of mRNA production lagged behind those of GtaC nuclear accumulation by about 3 to 3.5 min (Fig. 5). A delay is expected with this approach because of transcriptional initiation, elongation, and accumulation of transcripts that are necessary for observing the transcription "spot" (24). In contrast, cyclic transcription was not observed for $csaA$ in the absence of GtaC shuttling or for the housekeeping gene $act5$ even in the presence of robust GtaC shuttling (fig. S9, B to D). Therefore, via GtaC shuttling, the dynamics of external signals are transmitted internally and propagated to gene activation.

Next, we examined the impact of varying cAMP signaling inputs on the state and localization of GtaC. GtaC shuttling and its phosphocycling appeared to be synchronized to the rhythm of naturally occurring cAMP oscillations (Figs. 2E and 6A). When lower-frequency input was applied, GtaC responded once to each pulse (Fig. 6A). Conversely, with higher-frequency input, GtaC did not have sufficient time to be dephosphorylated and reenter the nucleus between pulses (Fig. 6A). This observation indicates that GtaC shuttling enables cells to track low-frequency, but filter out high-frequency, signals.

The ability to read and convert periodic cAMP signals into repeated gene activation predicts that the accumulation of GtaC-dependent gene products should increase with the number of consecutive cAMP pulses encountered by the cell rather than with developmental age. This was in fact the case for the expression of both $csaA$ and $cAR1$ (Fig. 6B and fig. S10A). Moreover, pulses at 6-min intervals, which mimicked the natural oscillation, led to higher levels of both gene products compared to less-frequent pulses (pulses at 12- and 20-min intervals), even when the cAMP concentration in each pulse was adjusted such that an equivalent total amount of stimuli was applied under different conditions (Fig. 6, C and D, and
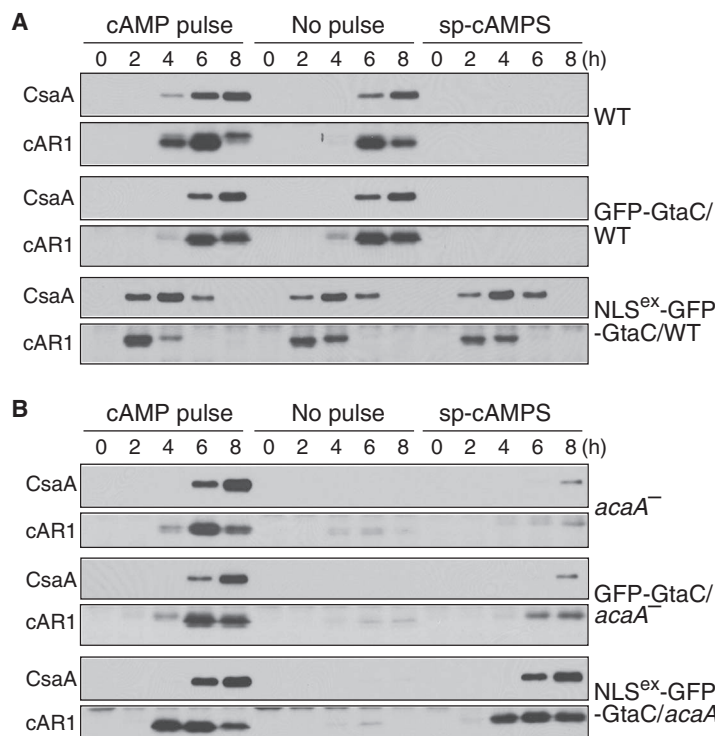
Fig. 4. The dual effects of cAMP during development. Cells were developed under different conditions, and samples were collected at the indicated time points and processed for Western blot analysis. (**A**) In WT and GFP-GtaC/WT cells, CsaA and cAR1 were induced by repeated cAMP stimuli (cAMP pulse), which reinforce natural oscillations (no pulse), but were suppressed by continuous stimulation (sp-cAMPS). Expressing NLS^{ex}-GFP-GtaC bypassed the inhibitory effect of sp-cAMPS. (**B**) In $acaA^-$ and GFP-GtaC/$acaA^-$ cells, the expression of CsaA and cAR1 required cAMP pulses (cAMP pulse). With NLS^{ex}-GFP-GtaC, either pulsatile (cAMP pulse) or continuous stimulation (sp-cAMPS) was effective in promoting gene expression, but NLS^{ex}-GFP-GtaC alone (no pulse) was not sufficient.

fig. S10, B and C). In contrast, stimuli that were too frequent to permit GtaC shuttling (Fig. 6A) were filtered out, as predicted, and resulted in little gene expression (Fig. 6C and fig. S10B). These experiments imply the existence of a "counting" mechanism involving GtaC shuttling that ensures gene expression to be properly tuned to the dynamics of cAMP input.

The dual effects of cAMP—it is required for gene expression but drives the key transcription factor, GtaC, out of the nucleus—suggest possible models for the counting mechanism. For example, the activation signal from cAMP could act in concert with GtaC before its exit from the nucleus (Fig. 6E). In this scenario, for a brief time during the rising phase of stimulation, gene expression would be activated and repeated stimuli would lead to reoccurring gene activations. This design resembles the positive edge trigger logic circuit that is frequently used as counter (Fig. 6E). Other similar models may also work. For example, the positive effect of cAMP could set in after GtaC leaves the nucleus and persist for a brief time after GtaC returns to the nucleus. To test the feasibility of using the positive edge trigger circuit to model GtaC-mediated gene expression responses, we carried out computer simulations. We modeled GtaC to be in one of three states: cytosolic (C), nuclear inactive (N), and nuclear active (N*). For simplicity, we assumed that the positive effect of cAMP acted directly on GtaC. Thus, the activation of GtaC (N→N*) and the inhibition of its nuclear localization (⊥C→N) were both regulated by G protein–coupled receptor (GPCR)–mediated processes. The increment of gene products during each stimulation cycle and general turnover rates were incorporated to account for the total level of expression under a given stimulus routine (detailed description is included in the supplementary materials). The simulations successfully recapitulated experimental observations. Transcriptional activation and the accumulation of gene product displayed the same frequency selectivity, with optimal expression occurring with correctly timed stimuli (Fig. 6, F and G).

Discussion

The results presented here reveal a unique mechanism by which oscillatory external signals are used to guide gene expression (Fig. 6H). Surface receptors including GPCRs have been shown to regulate transcriptional response. However, differing from most known examples, in the system we describe here, receptor occupancy leads to the nuclear exit, instead of entry, of the transcription factor. We show that this design can allow cAMP-driven, GtaC-mediated gene expression to occur in a distinct unit in response to each cycle of the repeated stimuli. Consequently, cells are able to count the number of effective stimuli they experience and respond with an appropriate level of gene expression.

Our findings provide several insights critical to the understanding of *Dictyostelium* biology. First, because cAMP waves organize cell aggregation, having gene expression dependent on the number rather than on the absolute concentration

of cAMP stimuli coordinates differentiation among a large population of cells over an expanded territory. Second, in early development, cAMP oscillations have a period similar to that of GtaC phosphocycles. This alignment may be evolutionarily selected because a phospho-cycle deviating from the natural frequency of cAMP oscillations compromises gene expression. Alternatively, the two systems may share regulatory components that keep them synchronized. Third, it is known that the frequency of cAMP oscillations progressively increases as development enters the mound stage (*25*), which corresponds nicely to a fall in the number of cells with nuclear enrichment of GtaC (movie S2). Thus, the "low-pass filter" property of the system to admit only low-frequency stimuli may allow the gene expression program to properly transition into the next developmental stage. Future studies are needed to reveal in finer detail the molecular mechanism underlying the dynamic regulation of GtaC and to understand how GtaC shuttling influences the expression of individual genes.

Oscillations at varying temporal and spatial scales are being increasingly observed in biological systems. These rhythmic phenomena regulate many important aspects of cell physiology. Adding to previous reports on oscillatory actions in other systems (*18*, *19*, *26–31*), pulsing may represent a

general mechanism for gene expression regulation. It will be interesting to find out whether mechanisms similar to the one we describe here operate in other circumstances where gene expression needs to be synchronized spatiotemporally among cell population or linked to repeated experience.

Materials and Methods

Cell Growth and Differentiation

Wild-type and gene deletion cell lines were cultured axenically in HL5 supplemented with antibiotics (*32*). Cells carrying expression constructs were maintained in HL5 containing G418 (10 to 20 μg/ml) or hygromycin (50 μg/ml). Developmental assays were performed as described previously with exponentially growing cells (*32*). Briefly, for development on bacterial lawn, cells were diluted in HL5 without antibiotics and plated with a suspension of *Klebsiella aerogenes* on SM plate. For development on non-nutrient agar, cells were washed with developmental buffer (DB) and plated on solidified DB agar at a density of 5.2 × 10^5 cells/cm^2. For most experiments, development in suspension was carried out by pulsing cells resuspended in DB at 2 × 10^7 cells/ml with 50 to 100 nM cAMP every 6 min starting from 1 hour. For the experiments presented in Fig. 6 (A to D)
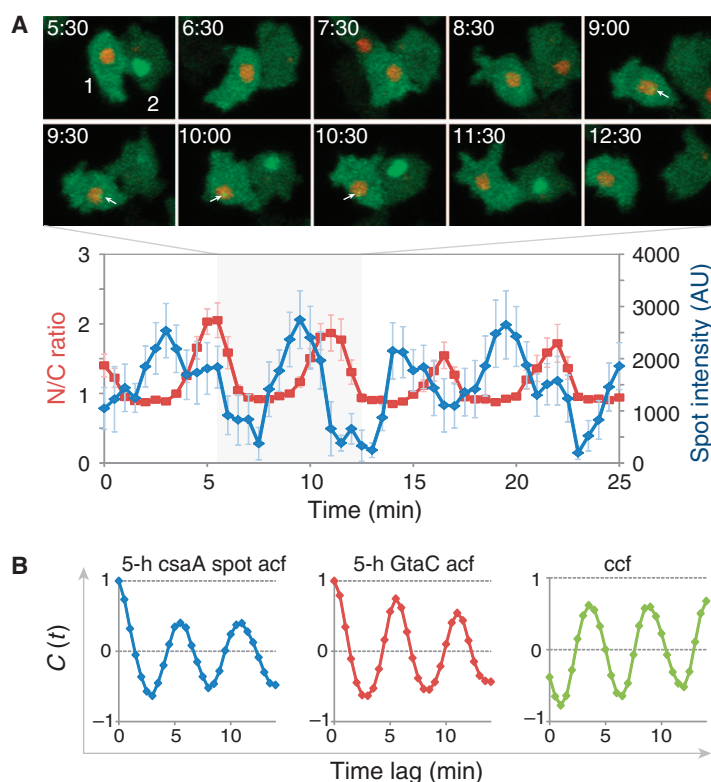
Fig. 5. GtaC shuttling promotes cyclic transcription. (**A**) Two populations of cells were mixed together to observe GtaC localization and transcription dynamics simultaneously. (Top) Image sequence (maximum intensity projections of three-dimensional stacks) showing GtaC translocation and *csaA* transcription in 5-hour (poststarvation) cells at the indicated time points. Cell 1, WT cell, in which an array of MS2 loops was integrated at the 5′ end of the *csaA* gene, stably expressing MS2-GFP and mRFP-H2B; cell 2, WT cell expressing GFP-GtaC. Transcription was visualized as a green spot (arrows) in the red nucleus. (Bottom) Quantification of the nucleus/cytoplasm fluorescence intensity ratio (N/C) of GFP-GtaC (*n* = 10) and the intensity of the *csaA* transcription spot (*n* = 12). Data are means ± SEM. (**B**) Autocorrelation (acf) and cross-correlation (ccf) plots.

and fig. S10 (A to C), *crac⁻* or GFP-GtaC/*crac⁻* cells were pulsed with different concentrations of cAMP or at different intervals starting from 2 hours. For development in the presence of sp-cAMPS, 1 μM was included in DB or DB agar.

Gene Disruption

The *gtaC⁻* cell line was generated from the Ax2 background. The disruption construct consists of a blasticidin S resistance (BSR) cassette from

pLPBLP (*33*) flanked by two genomic DNA fragments amplified by polymerase chain reaction (PCR) using primers KOF1-KOR1 and KOF2-KOR2, respectively (see table S2 for primer sequences). Through homologous recombination, the region of *GtaC* between +541 and +1323, in which +1 is the first and +2007 is the last nucleotide of the open reading frame, was replaced by the BSR cassette. Knockouts were screened by PCR and confirmed by Southern blotting.

Plasmid Construction

To generate constructs in which GtaC was tagged with GFP or Flag at the N terminus, full-length GtaC was amplified by PCR from genomic DNA using P1 and P2 primers, the two introns were subsequently deleted, and the resulting fragment was cloned into the Bgl II and Spe I sites in pDM317 or pDM320 (*34*). For deletion studies, N- and C-terminal fragments of GtaC were amplified by PCR and cloned into the Bgl II and Spe I
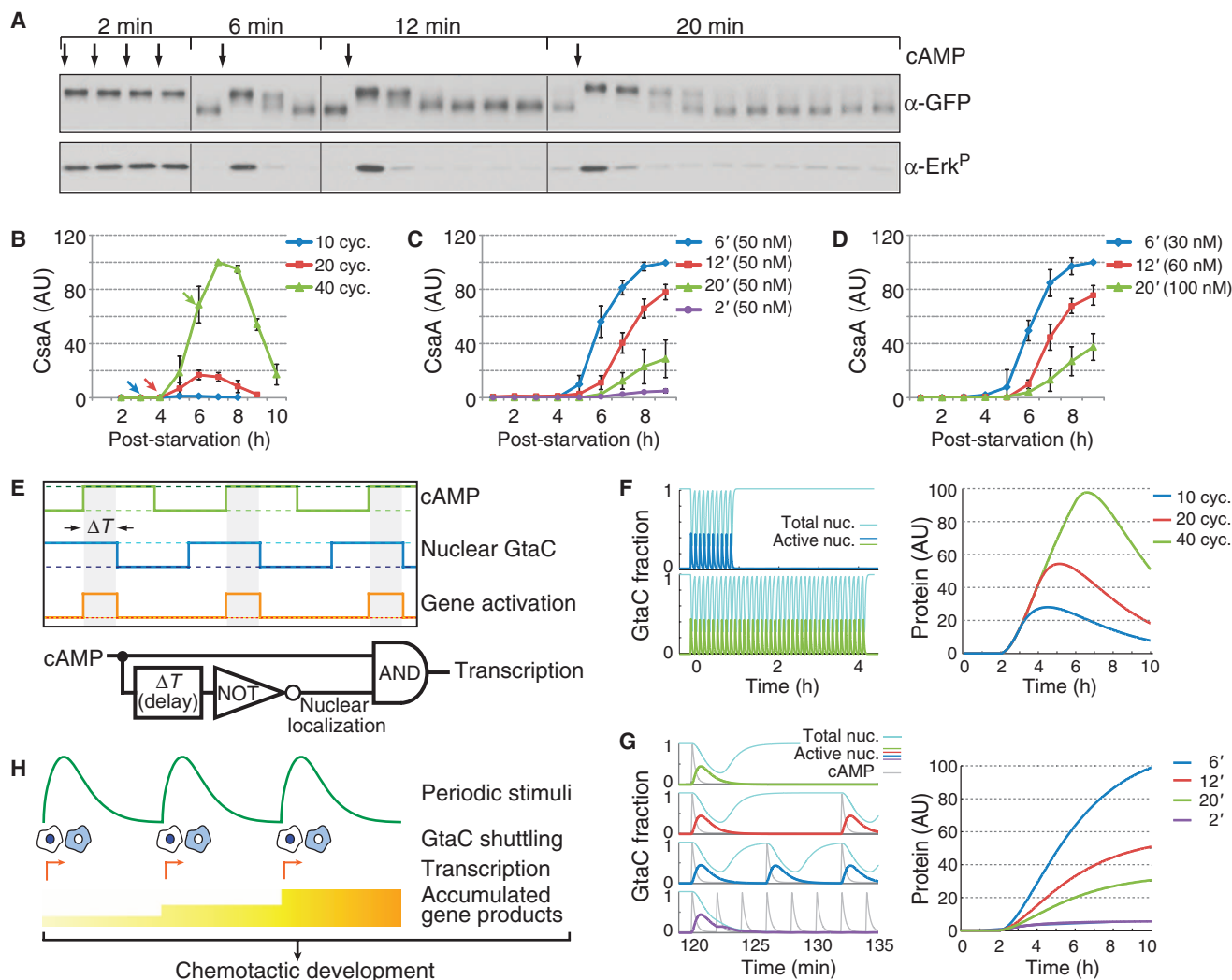
Fig. 6. GtaC shuttling constitutes a cellular mechanism that processes oscillatory cAMP signaling. (**A**) GFP-GtaC/*crac⁻* cells were developed with cAMP pulses applied at different intervals. Samples were collected every 2 min. (**B**) Expression of CsaA protein in *crac⁻* cells in response to different numbers of cAMP pulses applied at 6-min intervals. Arrows indicate the time points when pulses were discontinued. (**C**) Expression of CsaA in *crac⁻* cells in response to stimulations applied at different intervals. (**D**) Similar experiment as in (C) except that the cAMP concentration in each pulse was adjusted to generate an equivalent total amount of stimuli under different conditions. (**E**) (Top) A proposed model for cAMP-driven GtaC-mediated gene activation. In each cycle of stimulation (green line), the positive effect of cAMP on gene activation precedes the exit of GtaC from the nucleus (blue line), thereby creating a window of time (ΔT, gray shade) when both factors are present to promote gene expression (orange line). Persistent stimulation (dark green dashed line) drives GtaC out of the nucleus (dark blue dashed line), whereas lack of stimulation (light green dashed line) fails to generate an activation signal, and in both cases, gene expression is not activated (red and yellow dashed lines). This design resembles the "positive edge trigger" logical circuit. The biological circuit

consists of an AND gate with cAMP and nuclear GtaC as two inputs to activate transcription and a delayed NOT gate, by which cAMP controls the nuclear-to-cytoplasmic translocation of GtaC. The circuit becomes active when cAMP level goes from low to high. (**F**) Simulation showing the effects of the number of cAMP pulses. Ten, 20, or 40 pulses were applied, 6 min apart starting at 2 hours. (Left) Fractions of GtaC in the nucleus and active for 10 (top) and 40 (bottom) pulses. (Right) Protein expression as a function of time. The amount of protein is normalized to the total amount produced by a single pulse. (**G**) Simulation showing the effects of the pulsing period. Pulses spaced 2, 6, 12, and 20 min apart were applied starting at 2 hours. (Left) cAMP and fractions of GtaC in the nucleus and active. The peak concentration of cAMP is ~4 μM. (Right) Protein expression as a function of time. Note that with 2-min periods, the new pulse was applied before the GtaC reentered the nucleus; hence, the subsequent pulses did not lead to further activity. (**H**) Schematic of chemotactic development regulation. Repeated stimuli coupled with nucleocytoplasmic shuttling of GtaC generate units of transcription. Integration of sequential transcriptional activities allows cells to reckon the experience of stimulation and tune the level of gene expression.

sites in pDM448 and pDM317, respectively (34). To generate GFP-GtaC^{C-S}, the cysteine residues at positions 500, 503, 522, and 525 were mutated to serines. To generate GFP-GtaC$^{\Delta NLS}$, the region containing residues 468 to 496 was deleted. To generate GFP-GtaC^{KR-A}, lysines at positions 469, 470, 494, and 496 and arginines at positions 468 and 471 were mutated to alanines. To generate GtaC construct carrying mutations in the consensus PKA recognition sites, S^{472} and T^{473} were mutated to alanines. To generate GFP-GtaC^{3A}, T^{376}, S^{379}, and S^{380} were mutated to alanines. To generate NLS^{ex}-GFP-GtaC, DNA fragment amplified by PCR using primers P2 and P3 was cloned into the Bgl II and Spe I sites in pDM304 (34). To generate Flag-GskA, full-length GskA was amplified by PCR from genomic DNA using P4 and P5 primers and cloned into the Bgl II and Spe I sites in pDM320.

cAMP Stimulation and Immunoblotting

For the experiments presented in Fig. 2 (C and G) and fig. S5 (A, D, and E), cells developed in suspension for 2 hours were washed with cold DB, resuspended in DB to a density of 2×10^7 cells/ml, and kept on ice before stimulation. Cells were stimulated at room temperature with the addition of cAMP with a final concentration of 1 µM (Fig. 2, C and G, and fig. S5, D and E) or ranging from 0.3 to 300 nM (fig. S5A), lysed with 3× sample buffer, and boiled for 5 min. For the experiments presented in Fig. 2 (E and H) and fig. S5C, cells developed in suspension for 2.5 to 3 hours were collected right before or at different time points after the addition of one pulse of cAMP, lysed with 3× sample buffer, and boiled for 5 min. Combining with mutations in the zinc finger domain allowed us to examine the phosphorylation status of GtaC^{3A} and GtaC^{S472AS473A} in the wild-type background without compromising development or cell responsiveness to cAMP. To best observe the mobility shift of GtaC, proteins were separated on a 7.5% tris-HCl polyacrylamide gel (Criterion; Bio-Rad) and run at a constant voltage of 150 V for 110 min. To check the expression of CsaA and cAR1, cells were collected during development, pelleted, resuspended in DB to a final concentration of 5×10^7 cells/ml, and lysed with 3× sample buffer without boiling. Proteins were separated on a 4 to 15% tris-HCl polyacrylamide gel.

Western blotting was carried out as described previously (35). Equal protein loading was verified by staining the membrane with Coomassie Brilliant Blue after immunoblotting. We obtained antibody to GFP (catalog no. 11814460001) from Roche, antibody to phospho-serine (catalog no. 05-1000) from Millipore, and antibody to phospho-threonine (catalog no. 9381) from Cell Signaling Technology. Antibody to phospho-p44/42 MAPK (catalog no. 4370) from Cell Signaling Technology was used to detect phosphorylation of the ErkB kinase. Antibody to CsaA (33-294-17-s) was from the Developmental Studies Hybridoma Bank.

Micropipette Assay

gtaC$^-$ cells expressing GFP-GtaC or NLS^{ex}-GFP-GtaC were developed on the surface of non-nutrient agar. Differentiated cells were diluted in DB, plated on coverslip chambers (Lab-Tek, Nalge-Nunc), allowed to adhere for ~10 to 15 min, covered with DB, and then exposed to a micropipette filled with 10 µM cAMP. Chemotaxis was recorded by time-lapse video using an inverted microscope (Zeiss Observer.Z1) with a 10×/0.3 objective. Images were acquired at 30-s intervals using the AxioVision software. Motility speed and chemotaxis index were measured as described previously (36).

Image Acquisition

For the experiments presented in Fig. 1A and fig. S2A, GFP-GtaC/gtaC$^-$ cells were plated on a chambered coverslip at a density of 3.5×10^5 cells/cm^2 and submerged in DB. After 3 to 3.5 hours, time-lapse video was obtained using a Yokogawa CSU10 spinning disc confocal microscope equipped with a 40×/0.3 oil objective. Images were acquired at 30-s intervals using the SlideBook software. For the experiments presented in fig. S3, cells were washed with DB and plated on the surface of a thin layer of DB agar in a one-well coverslip chamber at a density of 4.5×10^5 cells/cm^2. Time-lapse video was taken at 4 hours using a Zeiss Observer. Z1 inverted microscope equipped with a 10×/0.3 air objective. Images were acquired at 1-min intervals with GFP illumination.

For the experiments presented in Figs. 1D and 2 (A and B) and figs. S4B, S5G, and S6A, cells developed in suspension for 2 hours were collected, washed, and diluted in DB. Cells (360 µl) at a density of 1.4×10^5 cells/ml were plated in an eight-well coverslip chamber. Cells were allowed to adhere for 10 to 15 min. Forty microliters of 1 µM cAMP was added for stimulation. For the "remove cAMP" experiment presented in Fig. 1D, cells were first stimulated as described above, and the stimulus was applied for at least 5 min for the nuclear-to-cytoplasmic translocation to complete. Imaging started when the stimulus was replaced with DB. GtaC relocalization was captured by time-lapse video using an UltraView spinning disc confocal microscope (DM 16000; PerkinElmer) equipped with a 40×/1.25–0.75 oil objective. Images were acquired at 20-s intervals using the SlideBook software.

For the experiments presented in Fig. 2I and fig. S2C, cells were developed in suspension for 2.5 hours. Cells were collected right before or at different time points after the addition of one pulse of cAMP (100 nM) and fixed immediately in phosphate-buffered saline (PBS) containing 3.7% formaldehyde. Fixed cells were washed once with PBS and plated on a chambered coverslip. Images were acquired using the SlideBook software on a Yokogawa CSU10 spinning disc confocal microscope equipped with a 40×/0.3 oil objective.

For the experiments presented in fig. S8 (B and C), cells were developed under different conditions and plated in an eight-well coverslip chamber. Images were acquired with phase illumination on a Zeiss Observer.Z1 inverted microscope equipped with a 20×/0.3 air objective.

To visualize transcription of csaA and act5, MS2 knock-in cells were cotransformed with plasmids encoding MS2-GFP that binds to nascent mRNA at the transcription site and mRFP-H2B that labels the nucleus (24). To image transcription and GtaC simultaneously, MS2-GFP + mRFP-H2B/wild-type and GFP-GtaC/wild-type cells were washed with KK2 buffer (20 mM potassium phosphate, pH 6.2), and equal numbers of cells were mixed and plated on 2% of KK2 agar at a density of 3.5×10^5 cells/cm^2. After 7 min for cells to settle, the buffer was removed and the cells were incubated in a humidified chamber. Agar was inverted onto an imaging dish before imaging and covered with mineral oil to prevent desiccation. Cells were captured using an A1R resonant scanning confocal microscope (Nikon) equipped with a 60×/1.49 oil objective and a controllable XY stage with a piezo attachment for rapid three-dimensional capture at multiple xy positions. Three-dimensional stacks (35 slices; 350-nm z step) were captured every 30 s for 25 min.

Image Analysis

ImageJ [National Institutes of Health (NIH)] was used for most analyses. To quantitate fluorescence intensity at single-cell level as presented in Figs. 1 (B and D) and 2B and figs. S2B, S5G, and S6A, the background-corrected mean pixel intensity of the nuclear and/or the cytoplasmic region was measured. To generate the histogram presented in Fig. 1B, the nucleus/cytosol ratios from 20 cells were binned to ranges of 0.5 intervals, and the frequency of each ratio range was plotted. For graphs presented in Fig. 2I and fig. S2C, the percentage of cells with greater nucleus/cytosol intensity ratio was determined. For quantification of length/width ratio as presented in fig. S8 (B and C), the distance from the leading edge, as defined by the front of protrusions, to the trailing tail was taken as cell length, and the width of the leading edge, as cell width.

To quantitate the period of nuclear intensity oscillations as presented in Fig. 1C, the response of the cell population as a whole was captured by measuring the average fluorescence intensity over the entire image using a similar method described previously (25). Briefly, the original images from movie S1 were processed with the smooth function in ImageJ. The smoothed images were then subtracted from the original images. The average intensity of all pixels of the resultant images was calculated and plotted against time. Higher intensities correspond to images in which most cells showed nuclear enrichment of GFP-GtaC. Peaks of the intensity plot were interpolated from the zero points of the difference plot, and the intervals between peaks were used to calculate the periodicity. To quantitate speed of movement for Fig. 1C and fig. S2B, images were analyzed using the MTrackJ plug-in (E. Meijering, Erasmus MC, University Medical Center Rotterdam) to generate velocity data. Cells that moved out of the imaging field during the movie were excluded for analysis. In Fig. 1C, the average velocity of 10 cells was plotted against time.

To quantitate fluorescence intensities at the transcriptional sites for Fig. 5 and fig. S9 (B to D), Velocity 3D Image Analysis Software (PerkinElmer)

was used to detect spots and measure intensity values. Only cells that stayed entirely within the imaging field during the movie were analyzed. Background intensities were measured from $5 \times 5 \times 5$ voxel cubes applied to cell bodies. Spot intensities at transcriptional sites were calculated after background subtraction. The temporal autocorrelation function of GtaC and the transcriptional spot are given by the following equation

$$C(t) = \frac{(I(t) - \mu) \cdot (I(0) - \mu)}{\sigma^2}$$

where $I(t)$ is the N/C ratio of GtaC fluorescence intensity or the fluorescence intensity of the transcriptional spot at time t, and μ and σ are the mean and SD, respectively, of each. The temporal cross-correlation function is given by the following equation

$$C_{\text{GtaC--Spot}}(t) =$$
$$\frac{(I_{\text{GtaC}}(0) - \mu_{\text{GtaC}}) \cdot (I_{\text{Spot}}(t) - \mu_{\text{Spot}})}{\sigma_{\text{GtaC}} \sigma_{\text{Spot}}}$$

where $I_x(t)$ is the N/C ratio of GtaC fluorescence intensity or the intensity of the transcriptional spot at time t, and μ_x and σ_x are the mean and SD of I_x, where $x = $ GtaC or Spot. Because the period of spontaneous cAMP oscillations often varies, data were not averaged between experiments.

Statistical significance and P values ($P < 0.05$ was considered significant) were determined using the two-tailed Student's t test. Mean values ± either SD or SEM were reported as indicated in the figure legends. Statistics were derived from three independent experiments for Figs. 1D, 2 (B and I), 3A, and 6 (B to D) and figs. S2C, S5G, S6A, S8 (B and C), and S10.

Immunoprecipitation and Phosphatase Treatment

GFP-GtaC/$gtaC^-$ cells were collected before and after cAMP stimulation, lysed at a density of 2×10^7 cells/ml by adding equal volume of 2× lysis buffer [20 mM sodium phosphate (pH 7.2), 100 mM NaCl, 1% (v/v) NP-40, 100 mM NaF, 50 mM sodium pyrophosphate, 4 mM Na$_3$VO$_4$, 2× Complete EDTA-free protease inhibitor mixture (Roche, catalog no. 11873580001)], and incubated on ice for 5 min. Lysates were centrifuged at 16,000g for 5 min to remove debris. Supernatant (600 µl) was incubated with 10 µl of ChromoTek GFP-Trap beads (catalog no. ACT-CM-GFA0050) at 4°C for 2 hours. After washes with buffer [10 mM sodium phosphate (pH 7.2), 50 mM NaCl, 0.5% NP-40, 1× Complete EDTA-free protease inhibitor mixture], the beads were washed with and resuspended in 20 µl of phosphatase buffer (New England Biolabs, catalog no. P0753). Reaction was initiated by the addition of 0.5 µl of λ-protein phosphatase, allowed to proceed for 20 min at 30°C, and stopped by the addition of 15 µl of 3× sample buffer.

GskA Kinase Assay

To purify GtaC as the substrate, GFP-GtaC/$gskA^-$ cells were collected before and after cAMP stimulation, lysed at a density of 1×10^7 cells/ml by

adding equal volume of 2× lysis buffer [50 mM tris (pH 7.5), 200 mM NaCl, 1% NP-40, 100 mM NaF, 50 mM sodium pyrophosphate, 4 mM Na$_3$VO$_4$, 2× Complete EDTA-free protease inhibitor mixture], and incubated on ice for 5 min. One milliliter of cleared lysate was incubated with 30 µl of ChromoTek GFP-Trap beads at 4°C for 1.5 hours. Beads were washed with 1× lysis buffer and kept on ice before assay. To purify GskA, Flag-GskA/$gskA^-$ cells were washed with DB and lysed at a density of 2×10^7 cells/ml by adding equal volume of 2× lysis buffer. One milliliter of cleared lysate was incubated with 15 µl of anti-Flag M2 affinity resin (Sigma, catalog no. F2426) at 4°C for 3 hours. Beads were washed with 1× lysis buffer and elution buffer [25 mM tris (pH 7.5), 100 mM NaCl, 0.1% NP-40]. Flag-GskA was eluted by the addition of 100 µl of elution buffer containing 3× Flag peptide (300 ng/µl) (Sigma, catalog no. F4799) at 4°C for 30 min. For kinase reaction, 15 µl of GFP-GtaC–containing beads was washed with elution buffer and mixed with 40 µl of Flag-GskA–containing eluate. Reaction was initiated by the addition of 13× adenosine 5′-triphosphate (ATP) mix (130 mM MgCl$_2$, 65 mM DTT, 3.9 mM ATP), allowed to proceed for 15 min at room temperature, and stopped by the addition of protein sample buffer.

Limited Proteolysis

To purify phosphorylated and dephosphorylated forms of GtaC, Flag-GtaC/$gtaC^-$ cells were collected before and after cAMP stimulation. Cells (4×10^8) were lysed through two layers of 5-µm filter membranes (Whatman, catalog no. 110613) in the presence of 6× lysis buffer [120 mM tris (pH 8.5), 150 mM NaF, 6 mM Na$_3$VO$_4$, 75 mM sodium pyrophosphate, 6× Complete EDTA-free protease inhibitor mixture]. Lysates were centrifuged at 16,000g for 15 min to remove debris. Triton X-100, NaCl, and glycerol were added to the supernatant to a final concentration of 0.5% (v/v), 0.46 M, and 5% (v/v), respectively. The supernatant was then incubated with 90 µl of anti-Flag M2 affinity resin at 4°C for 3 hours. Beads were washed with washing buffer (1× lysis buffer, 0.5% Triton X-100, 0.46 M NaCl, 5% glycerol) and elution buffer [25 mM tris (pH 7.5), 0.4% Triton X-100, 100 mM NaCl]. Flag-GtaC was eluted by the addition of 300 µl of elution buffer containing 3× Flag peptide (300 ng/µl) at 4°C for 1 hour. Limited proteolysis with trypsin (Sigma, catalog no. T1426) was performed at a protein/protease mass ratio of 1000:1. The reaction was carried out at 37°C, and aliquots were removed at 10, 20, 30, 40, and 60 min. The reaction was stopped by the addition of 3× sample buffer and analyzed by SDS–polyacrylamide gel electrophoresis and silver staining.

Whole-Transcriptome RNA-Seq and Computational Analysis

Wild-type (Ax2), $gtaC^-$, GFP-GtaC/$gtaC^-$, and NLS^{ex}-GFP-GtaC/$gtaC^-$ cells were developed on DB agar in duplication. RNA samples were collected at 0, 1, 2, and 5 hours and processed as

described previously (37) with the following modifications to perform multiplexed sequencing. At the final step of library preparation, adaptor-ligated complementary DNAs were indexed by PCR using primers that contain a single specific 7-mer barcode. Every eight indexed samples were pooled, and Illumina-based multiplexed sequencing was performed. baySeq package was used to detect differentially expressed genes (38). GtaC-activated target candidates were identified among differentially expressed genes on the basis of two criteria: (i) expression in wild-type and GFP-GtaC/$gtaC^-$ cells at the indicated time point (1, 2, or 5 hours) is at least twofold higher than that in 0-hour wild-type cells; (ii) expression in $gtaC^-$ at the indicated time point (1, 2, or 5 hours) is at least twofold lower than that in wild-type and GFP-GtaC/$gtaC^-$ cells [false discovery rate (FDR) < 0.05 and likelihood > 0.90]. The precociously activated genes were identified as differentially expressed genes that meet the criteria (FDR < 0.05, likelihood > 0.90, and log$_2$ ratio > 1) in NLS^{ex}-GFP-GtaC/$gtaC^-$ cells compared to GFP-GtaC/$gtaC^-$ cells at time points before 5 hours. topGO package (version 2.14.0) was used to analyze GO term enrichment with the annotation file (November 2012) from dictyBase.

Computer Simulation of GtaC-Mediated Gene Activation

We consider GtaC to be in one of three states: cytosolic (C), nuclear inactive (N), and nuclear active (N^*). The activation of GtaC ($N \rightarrow N^*$) is regulated by a receptor-mediated process (E). Similarly, nuclear localization ($C \rightarrow N$) is inhibited by a second receptor-mediated process (I). Shuttling to the cytoplasm occurs at a constant rate but is limited to the active form of GtaC. Thus, concentrations of the three states are governed by the ordinary differential equations

$$\frac{dN}{dt} = k_1 \frac{C}{k_M + 1} \left(\frac{V_C}{V_N} \right) - k_2 N \cdot E$$
$$\frac{dN^*}{dt} = k_2 N \cdot E - k_3 N^*$$
$$\frac{dC}{dt} = k_3 N^* \left(\frac{V_N}{V_C} \right) - k_1 \frac{C}{k_M + 1}$$

Here, V_N and V_C correspond to the volumes of the nucleus and cytoplasm, respectively, and are required to correct for the varying effect that shuttling between the two compartments of different volumes has on concentrations. We assume that the volume of the nucleus is 1/24th that of the cytoplasm. Note that $N + N^* + C \left(\frac{V_C}{V_N} \right) = $ constant, which we can take to be one.

We assume that both E and I are regulated by cAMP receptor occupancy (U) as linear processes

$$\frac{dE}{dt} = k_E (U - E)$$
$$\frac{dI}{dt} = k_I (U - 1)$$

In these equations, receptor occupancy is normalized (ranging from 0 to 1), as are both E and I.

In particular, $U = \frac{\mathrm{cAMP}/K_D}{1+\mathrm{cAMP}/K_D}$, where K_D is in the order of 200 nM (*39*). The cAMP signal follows the following equation

$$\frac{\mathrm{dcAMP}}{\mathrm{d}t} = -k_\mathrm{d}\mathrm{cAMP} + \mathrm{cAMP}_\mathrm{app}(t)$$

where the applied cAMP signal is 1 μM = 5 K_D. The coefficient k_d represents the degradation of extracellular cAMP by phosphodiesterases, which happens with a half-life of about 10 s (*40*).

Finally, we model transcription and translation using the following differential equations

$$\frac{\mathrm{d}_M}{\mathrm{d}t} = -k_\mathrm{mRNA}M + N*$$
$$\frac{\mathrm{d}P}{\mathrm{d}t} = -k_\mathrm{prot}P + M$$

The coefficients k_mRNA and k_prot are chosen so that the half-lives of the mRNA and protein are 1 and 2 hours, respectively.

We selected the unknown parameters by minimizing a function that penalizes three things: the difference between the experimental and simulated concentrations of nuclear signal to both addition and removal of persistent stimuli, the concentration of active nuclear GtaC 200 s after application of a persistent stimulus, and (the inverse of) the peak nuclear GtaC after application of a persistent stimulus. The parameter search was carried out using the Matlab command fminsearch. The parameters used in the simulations are given in table S1.

References and Notes

1. P. E. Belchetz, T. M. Plant, Y. Nakai, E. J. Keogh, E. Knobil, Hypophysial responses to continuous and intermittent delivery of hypopthalamic gonadotropin-releasing hormone. *Science* **202**, 631–633 (1978). doi: 10.1126/science.100883; pmid: 100883
2. H. Shimojo, T. Ohtsuka, R. Kageyama, Oscillations in notch signaling regulate maintenance of neural progenitors. *Neuron* **58**, 52–64 (2008). doi: 10.1016/j.neuron.2008.02.014; pmid: 18400163
3. J. Mauelshagen, C. M. Sherff, T. J. Carew, Differential induction of long-term synaptic facilitation by spaced and massed applications of serotonin at sensory neuron synapses of *Aplysia californica*. *Learn. Mem.* **5**, 246–256 (1998). pmid: 10454368
4. D. S. Barkley, Adenosine-3',5'-phosphate: Identification as acrasin in a species of cellular slime mold. *Science* **165**, 1133–1134 (1969). doi: 10.1126/science.165.3898.1133; pmid: 4308325
5. T. M. Konijn, Y. Y. Chang, J. T. Bonner, Synthesis of cyclic AMP in *Dictyostelium discoideum* and *Polysphondylium pallidum*. *Nature* **224**, 1211–1212 (1969). doi: 10.1038/2241211a0; pmid: 4311588
6. N. Van Driessche et al., A transcriptional profile of multicellular development in *Dictyostelium discoideum*. *Development* **129**, 1543–1552 (2002). pmid: 11923193
7. N. Iranfar, D. Fuller, W. F. Loomis, Genome-wide expression analyses of gene regulation during early development of *Dictyostelium discoideum*. *Eukaryot. Cell* **2**, 664–670 (2003). doi: 10.1128/EC.2.4.664-670.2003; pmid: 12912885
8. G. Gerisch, B. Hess, Cyclic-AMP-controlled oscillations in suspended *Dictyostelium* cells: Their relation to morphogenetic cell interactions. *Proc. Natl. Acad. Sci. U.S.A.* **71**, 2118–2122 (1974). doi: 10.1073/pnas.71.5.2118; pmid: 4365764

9. C. Rossier, G. Gerisch, D. Malchow, Action of a slowly hydrolysable cyclic AMP analogue on developing cells of *Dictyostelium discoideum*. *J. Cell Sci.* **35**, 321–338 (1979). pmid: 217886
10. A. Kuspa, Restriction enzyme-mediated integration (REMI) mutagenesis. *Methods Mol. Biol.* **346**, 201–209 (2006). pmid: 16957292
11. H. Otsuka, P. J. Van Haastert, A novel Myb homolog initiates *Dictyostelium* development by induction of adenylyl cyclase expression. *Genes Dev.* **12**, 1738–1748 (1998). doi: 10.1101/gad.12.11.1738; pmid: 9620859
12. C. J. Lim, G. B. Spiegelman, G. Weeks, RasC is required for optimal activation of adenylyl cyclase and Akt/PKB during aggregation. *EMBO J.* **20**, 4490–4499 (2001). doi: 10.1093/emboj/20.16.4490; pmid: 11500376
13. K. J. Tomchik, P. N. Devreotes, Adenosine 3',5'-monophosphate waves in *Dictyostelium discoideum*: A demonstration by isotope dilution–fluorography. *Science* **212**, 443–446 (1981). doi: 10.1126/science.6259734; pmid: 6259734
14. P. N. Devreotes, M. J. Potel, S. A. MacKay, Quantitative analysis of cyclic AMP waves mediating aggregation in *Dictyostelium discoideum*. *Dev. Biol.* **96**, 405–415 (1983). doi: 10.1016/0012-1606(83)90178-1; pmid: 6299820
15. F. Alcantara, M. Monk, Signal propagation during aggregation in the slime mould *Dictyostelium discoideum*. *J. Gen. Microbiol.* **85**, 321–334 (1974). doi: 10.1099/00221287-85-2-321; pmid: 4615133
16. B. Wurster, U. Butz, A study on sensing and adaptation in *Dictyostelium discoideum*: Guanosine 3',5'-phosphate accumulation and light-scattering responses. *J. Cell Biol.* **96**, 1566–1570 (1900). doi: 10.1083/jcb.96.6.1566; pmid: 6304110
17. G. Lahav et al., Dynamics of the p53-Mdm2 feedback loop in individual cells. *Nat. Genet.* **36**, 147–150 (2004). doi: 10.1038/ng1293; pmid: 14730303
18. D. E. Nelson et al., Oscillations in NF-κB signaling control the dynamics of gene expression. *Science* **306**, 704–708 (2004). doi: 10.1126/science.1099962; pmid: 15499023
19. A. Hoffmann, A. Levchenko, M. L. Scott, D. Baltimore, The IκB-NF-κB signaling module: Temporal control and selective gene activation. *Science* **298**, 1241–1245 (2002). doi: 10.1126/science.1071914; pmid: 12424381
20. H. Hirata et al., Oscillatory expression of the bHLH factor Hes1 regulated by a negative feedback loop. *Science* **298**, 840–843 (2002). doi: 10.1126/science.1074560; pmid: 12399594
21. R. Teo et al., Glycogen synthase kinase-3 is required for efficient *Dictyostelium* chemotaxis. *Mol. Biol. Cell* **21**, 2788–2796 (2010). doi: 10.1091/mbc.E09-10-0891; pmid: 20534815
22. A. Parikh et al., Conserved developmental transcriptomes in evolutionarily divergent species. *Genome Biol.* **11**, R35 (2010). doi: 10.1186/gb-2010-11-3-r35; pmid: 20236529
23. J. R. Chubb, T. Trcek, S. M. Shenoy, R. H. Singer, Transcriptional pulsing of a developmental gene. *Curr. Biol.* **16**, 1018–1025 (2006). doi: 10.1016/j.cub.2006.03.092; pmid: 16713960
24. T. Muramoto et al., Live imaging of nascent RNA dynamics reveals distinct types of transcriptional pulse regulation. *Proc. Natl. Acad. Sci. U.S.A.* **109**, 7350–7355 (2012). doi: 10.1073/pnas.1117603109; pmid: 22529358
25. D. Dormann, G. Weijer, C. A. Parent, P. N. Devreotes, C. J. Weijer, Visualizing PI3 kinase-mediated cell-cell signaling during *Dictyostelium* development. *Curr. Biol.* **12**, 1178–1188 (2002). doi: 10.1016/S0960-9822(02)00950-8; pmid: 12176327
26. I. Imayoshi et al., Oscillatory control of factors determining multipotency and fate in mouse neural progenitors. *Science* **342**, 1203–1208 (2013). doi: 10.1126/science.1242366; pmid: 24179156
27. N. Hao, B. A. Budnik, J. Gunawardena, E. K. O'Shea, Tunable signal processing through modular control of transcription factor translocation. *Science* **339**, 460–464 (2013). pmid: 23349292
28. J. E. Purvis et al., p53 dynamics control cell fate. *Science* **336**, 1440–1444 (2012). doi: 10.1126/science.1218351; pmid: 22700930
29. R. E. Dolmetsch, K. L. Xu, R. S. Lewis, Calcium oscillations increase the efficiency and specificity of gene expression.

Nature **392**, 933–936 (1998). doi: 10.1038/31960; pmid: 9582075
30. L. Cai, C. K. Dalal, M. B. Elowitz, Frequency-modulated nuclear localization bursts coordinate gene regulation. *Nature* **455**, 485–490 (2008). doi: 10.1038/nature07292; pmid: 18818649
31. D. A. Stavreva et al., Ultradian hormone stimulation induces glucocorticoid receptor–mediated pulses of gene transcription. *Nat. Cell Biol.* **11**, 1093–1102 (2009). doi: 10.1038/ncb1922; pmid: 19684579
32. H. Cai, C. H. Huang, P. N. Devreotes, M. Iijima, Analysis of chemotaxis in *Dictyostelium*. *Methods Mol. Biol.* **757**, 451–468 (2012). doi: 10.1007/978-1-61779-166-6_26; pmid: 21909927
33. J. Faix, L. Kreppel, G. Shaulsky, M. Schleicher, A. R. Kimmel, A rapid and efficient method to generate multiple gene disruptions in *Dictyostelium discoideum* using a single selectable marker and the Cre-loxP system. *Nucleic Acids Res.* **32**, e143 (2004). doi: 10.1093/nar/gnh136; pmid: 15507682
34. D. M. Veltman, I. Keizer-Gunnink, P. J. Haastert, An extrachromosomal, inducible expression system for *Dictyostelium discoideum*. *Plasmid* **61**, 119–125 (2009). doi: 10.1016/j.plasmid.2008.11.003; pmid: 19046986
35. Y. Artemenko, K. F. Swaney, P. N. Devreotes, Assessment of development and chemotaxis in *Dictyostelium discoideum* mutants. *Methods Mol. Biol.* **769**, 287–309 (2011). doi: 10.1007/978-1-61779-207-6_20; pmid: 21748684
36. H. Cai et al., Ras-mediated activation of the TORC2–PKB pathway is critical for chemotaxis. *J. Cell Biol.* **190**, 233–245 (2010). pmid: 20660850
37. E. Huang et al., BzpF is a CREB-like transcription factor that regulates spore maturation and stability in *Dictyostelium*. *Dev. Biol.* **358**, 137–146 (2011). doi: 10.1016/j.ydbio.2011.07.017; pmid: 21810415
38. T. J. Hardcastle, K. A. Kelly, baySeq: Empirical Bayesian methods for identifying differential expression in sequence count data. *BMC Bioinformatics* **11**, 422 (2010). doi: 10.1186/1471-2105-11-422; pmid: 20698981
39. Z. Xiao, Y. Yao, Y. Long, P. Devreotes, Desensitization of G-protein-coupled receptors. agonist-induced phosphorylation of the chemoattractant receptor *cAR1* lowers its intrinsic affinity for cAMP. *J. Biol. Chem.* **274**, 1440–1448 (1999). doi: 10.1074/jbc.274.3.1440; pmid: 9880518
40. S. Bader, A. Kortholt, P. J. Van Haastert, Seven *Dictyostelium discoideum* phosphodiesterases degrade three pools of cAMP and cGMP. *Biochem. J.* **402**, 153–161 (2007). doi: 10.1042/BJ20061153; pmid: 17040207

Supplementary Materials

Science

AAAS

Nucleocytoplasmic Shuttling of a GATA Transcription Factor Functions as a Development Timer

Huaqing Cai *et al.*
Science **343**, (2014);
DOI: 10.1126/science.1249531